ALMA MATER STUDIORUM
UNIVERSITÀ DI BOLOGNA

ARCHIVIO ISTITUZIONALE
DELLA RICERCA

Alma Mater Studiorum Università di Bologna
Archivio istituzionale della ricerca

RTN Analysis of Schottky p-GaN Gate HEMTs Under Forward Gate Stress: Impact of Temperature

This is the final peer-reviewed author’s accepted manuscript (postprint) of the following publication:

Published Version:
Millesimo, M., Valentini, L., Fiegna, C., Sangiorgi, E., Tallarico, A.N., Borga, M., et al. (2025). RTN Analysis of Schottky p-GaN Gate HEMTs Under Forward Gate Stress: Impact of Temperature. NEW YORK : Institute of Electrical and Electronics Engineers Inc. [10.1109/IRPS48204.2025.10982856].

Availability:
This version is available at: https://hdl.handle.net/11585/1032557 since: 2025-12-15

Published:
DOI: http://doi.org/10.1109/IRPS48204.2025.10982856

Terms of use:

Some rights reserved. The terms and conditions for the reuse of this version of the manuscript are specified in the publishing policy. For all terms of use and more information see the publisher's website.

This item was downloaded from IRIS Università di Bologna (https://cris.unibo.it/).
When citing, please refer to the published version.

(Article begins on next page)

10 May 2026

This is the post-print peer-review accepted manuscript of:

M. Millesimo *et al.*, "RTN Analysis of Schottky p-GaN Gate HEMTs Under Forward Gate Stress: Impact of Temperature," *IEEE International Reliability Physics Symposium Proceedings,* Monterey, California, USA, 2025, pp. 8A-2.1 – 8A-2.7, DOI: 10.1109/IRPS48204.2025.10982856.

The published version is available online at:

https://ieeexplore.ieee.org/stamp/stamp.jsp?tp=&arnumber=10982856

© 2025 IEEE. Personal use of this material is permitted. Permission from IEEE must be obtained for all other uses, in any current or future media, including reprinting/republishing this material for advertising or promotional purposes, creating new collective works, for resale or redistribution to servers or lists, or reuse of any copyrighted component of this work in other works.

RTN Analysis of Schottky p-GaN gate HEMTs Under Forward Gate Stress: Impact of Temperature

M. Millesimo*, L. Valentini, C. Fiegna, E. Sangiorgi, A.N. Tallarico,
Advanced Research Center on Electronic System – Department of Electrical, Electronic, and Information Engineering "Guglielmo Marconi"
University of Bologna
Campus of Cesena, Cesena, Italy
* e-mail: maurizio.millesimo2@unibo.it

M. Borga, N. Posthuma, S. Decoutere
imec - interuniversitair micro electronica centrum
Kapeldreef 75, Heverlee, Belgium

B. Bakeroot
Centre for Microsystems Technology, imec and Ghent University
9052 Ghent, Belgium

***Abstract*— This study presents a comprehensive analysis of random telegraph noise (RTN) to evaluate the impact of forward gate bias (V_{GS}) and temperature (T) on defects creation and activation in the gate epi-stack of GaN-based Schottky p-GaN gate HEMTs. Results reveal three RTN components in the fresh device currents at elevated temperatures (90 °C to 150 °C), attributed to pre-existing defects within the AlGaN barrier, influencing both the gate leakage and the drain current. Temperature-dependent RTN analysis is used to extract the activation energies of these traps. Conversely, no RTN components are observed in fresh device currents at lower temperatures (≤ 70 °C), highlighting the role of thermal excitation in defects activation. Under forward gate stress, four additional RTN components emerge, suggesting new traps formation. Findings highlight the combined roles of temperature and V_{GS} in activating pre-existing defects and inducing new ones within the gate epi-stack of Schottky p-GaN gate HEMTs.**

***Index Terms*-- Gallium Nitride, Defects Characterization, p-GaN HEMTs, Reliability, Trapping Mechanisms, Random Telegraph Noise, RTN Analysis.**

I. Introduction

Schottky p-GaN gate high-electron-mobility transistors (HEMTs) have gained significant importance in power electronics due to their unique properties, which address critical challenges in high-efficiency power conversion and high-speed switching applications [1]-[6]. Their relevance stems from the combination of superior material properties of GaN, as well as its alloys, and the p-GaN gate structure, which enable higher efficiency, improved performance and reliability, and reduced system size and cost compared to traditional silicon-based counterparts. These advantages make Schottky p-GaN gate HEMTs a cornerstone technology for next-generation power systems across a wide range of applications.

Given the growing interest in Schottky p-GaN gate HEMTs, extensive research has been dedicated to identifying the root causes of gate lifetime limitations and threshold voltage instability [6]-[18]. For these devices, reliability challenges are predominantly attributed to charge trapping phenomena or the formation of new traps within the p-GaN/AlGaN/GaN gate epi-stack, particularly under the combined influence of high gate overdrive and elevated temperatures [6]. To better understand the factors influencing device performance and long-term stability, it is crucial to gain deeper insights into the nature, localization, and dynamic behavior of these defects.

For a wide range of semiconductor devices, RTN analysis has proven to be a powerful method for localizing and characterizing defect states responsible of phenomena such as threshold voltage instability [19]-[26]. RTN components appear as sudden, unpredictable fluctuations between discrete levels in device currents and, in the frequency domain (power spectral density, PSD), they follow a Lorentzian spectrum with a $1/f^2$ trend [26]. This phenomenon is caused by the random capture and release of charge carriers by defect states. Although RTN analysis has been extensively studied across different technologies [24], only a few studies focus specifically on GaN-based Schottky pGaN gate HEMTs [27]-[28].

Recently, we reported a detailed investigation of RTN components under stress conditions induced by the application of a high gate voltage (V_{GS} = 9 V) at T = 25 °C [28]. This analysis led to the identification and characterization of four distinct RTN components. Three of these components were observed to simultaneously affect both the gate leakage (I_G) and the drain current (I_D), suggesting the creation/activation of defects within the AlGaN barrier. The simultaneous impact on both I_G and I_D indicates that these defects play a dual role in altering the gate leakage behavior and the threshold voltage. In contrast, the fourth RTN component was exclusively detected

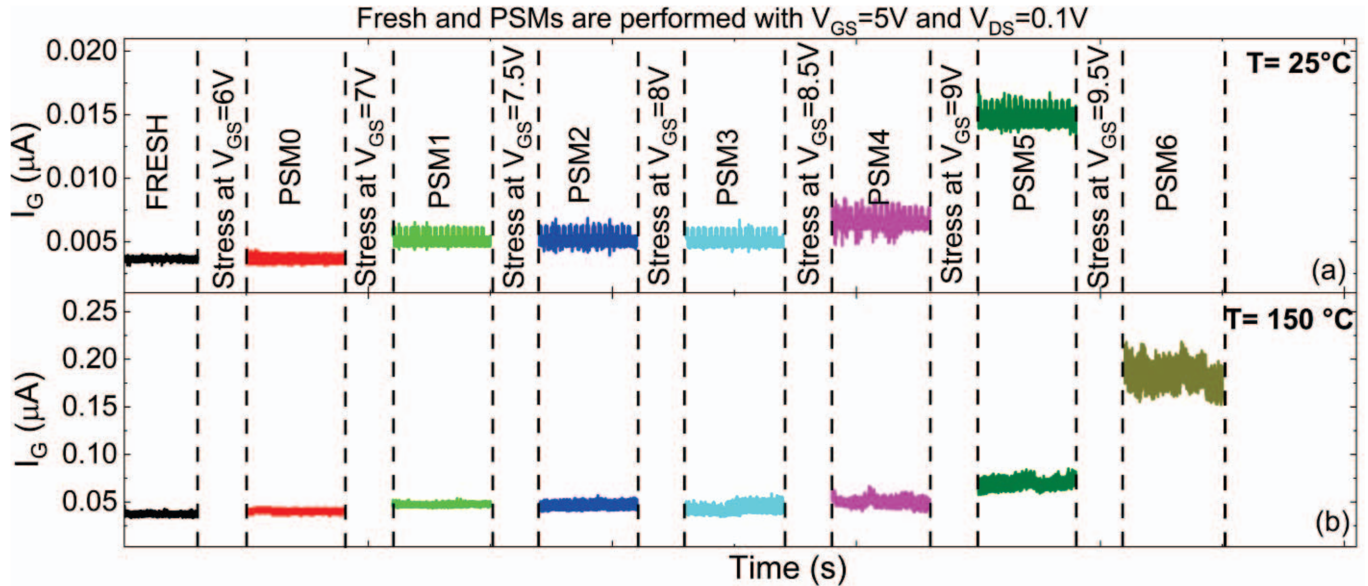

Figure 1. Post-stress measured gate currents at T=25 °C (a) and T=150°C (b) with V_{GS}=5V and V_{DS}=0.1V.

in the gate current and showed no measurable effect on the drain current, suggesting that the defect responsible for this RTN component is localized near the Schottky junction rather than being distributed throughout the AlGaN barrier.

In this study, the investigation is extended to provide a comprehensive analysis across a wider range of temperatures and gate-to-source voltages. This extended analysis offers deeper insights into the influence of these parameters on the creation and activation of traps within the gate epi-stack Schottky pGaN gate HEMTs. By systematically varying temperature and V_{GS}, the study explores the roles of thermal and electrical stress mechanisms in driving defect formation and activation, offering a more detailed understanding of defect dynamics under various operating conditions.

II. Device Struture and Stress Procedure

The devices under test (DUTs) are lateral GaN-based HEMTs with a metal/p-GaN Schottky gate structure, designed to achieve enhancement-mode operation. These transistors are fabricated at IMEC on 200-mm Silicon (Si) substrates. The vertical epitaxial structure built on top of the Si substrate, consists of a 200-nm AlN nucleation layer, a 1.65-µm AlN/GaN superlattice buffer layer, a 1-µm carbon-doped GaN back barrier, a 200-nm unintentionally doped GaN channel layer, a 16-nm AlGaN barrier layer with 23.5% aluminum content, and an 80-nm Mg-doped p-GaN layer, with a dopant concentration of 3×10^{19} cm^{-3}. For this study, symmetric devices are used, characterized by equal gate-to-source (L_{GS}) and gate-to-drain (L_{GD}) distances of 1.25 µm. The gate geometry is defined by a width (W_G) of 10 µm and a length (L_G) of 0.5 µm.

The measurement of both gate and drain currents, aimed at detecting RTN components, is performed using a two-channel Keysight Waveform Generator/Fast Measurement Unit (WGFMU) B1531A, which allows relatively short sampling intervals (as low as 10 µs).

A typical measure-stress-measure (MSM) technique has been employed to conduct a detailed analysis of RTN dynamics. In particular, the measurement/monitoring phases involve performing multiple sequential acquisitions of both gate and drain current, using a gate-to-source voltage (V_{GS}) of 5 V and a drain-to-source voltage (V_{DS}) of 0.1 V. To ensure comprehensive data capture, the sampling times were systematically varied from 10 µs to 10 ms, resulting in an aggregate measurement duration of approximately 8 x 10^4 s. These acquisitions were initially carried out on a fresh device and subsequently repeated after each stress phase, in which the stress voltage (V_{GS} > 5 V) is applied for 100 s. Following a step-stress approach, after each RTN monitoring phase, the stress voltage is increased up to device breakdown. The latter is identified by a sudden and significant increase in gate leakage current, exceeding 1 mA/mm. This approach allowed for systematic exploration of the relationship between applied gate bias and RTN behavior. For clarity, the post-stress measurements (PSMs) conducted after each stress phase are distinctly labeled. Specifically, the measurements corresponding to stress phases with V_{GS} values of 6 V, 7 V, 7.5 V, 8 V, 8.5 V, 9 V, and 9.5 V are designated as PSM0, PSM1, PSM2, PSM3, PSM4, PSM5, and PSM6, respectively. Furthermore, the temperature has been varied across a wide range, from 25 °C to 150 °C, to evaluate the temperature dependence of RTN characteristics and its correlation with defects behavior.

Figure 1 shows parts of the fresh and PSMs of I_G at 25 °C (a) and 150 °C (b). To ensure a better visualization, the x-axis is not in scale because of significant differences between stress and PMS times, i.e., 100 s and 8 x 10^4 s, respectively. In both cases, the I_G, monitored at V_{GS} = 5 V, increases with each stress phase. This consistent rise in gate leakage current indicates progressive damage to the gate epitaxial stack, likely resulting from the stress-induced degradation mechanisms.

III. Random Telegraph Noise Analysis

A. High Temperature

Figure 2 shows I_G and I_D measured at V_{GS} = 5 V and V_{DS} = 100 mV on the fresh device at a test temperature of 150 °C. It

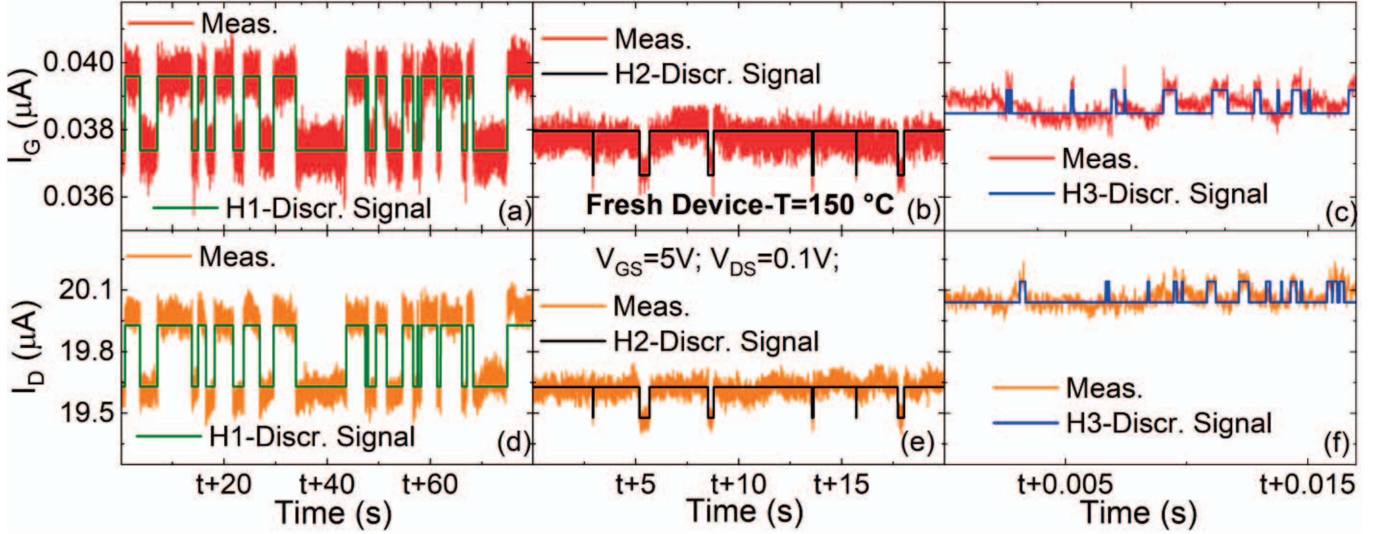

Figure 2. RTN and discretized waveform observed on I_G related to H1 (a), H2 (b) and H3 (c) on the fresh device at T=150 °C. Same RTN components are observable on their I_D (d), (e) and (f) for H1, H2 and H3, respectively.

is important to note that the reported data represent only a selected portion of the full data acquisition, with a focus on a shorter time window for clearer visualization of the current dynamics. Significant fluctuations between two distinct levels (RTN) are clearly observed in both currents. Unlike the behavior observed at room temperature [28], the fresh device currents at 150 °C exhibit three distinct RTN components, labeled H1, H2, and H3. Each component differs in amplitude and duration, suggesting the presence of pre-existing thermally activated defects within the AlGaN barrier. These defects likely reside at different spatial locations and/or energy levels within the AlGaN bandgap, as evidenced by the simultaneous fluctuations in both I_G and I_D.

The characterization of these defect-related RTN components is carried out following the post-processing procedures described in [28]. Initially, the RTN signals are discretized to isolate individual RTN signals for further analysis. The resulting discretized waveforms, shown in Fig. 2 (a), (b), and (c), correspond to the RTN components observed in I_G, attributed to traps H1, H2, and H3, respectively. The RTN components present in I_D have been discretized using the gate signal as a reference, with the corresponding waveforms shown in Fig. 2 (d), (e), and (f) for traps H1, H2, and H3, respectively.

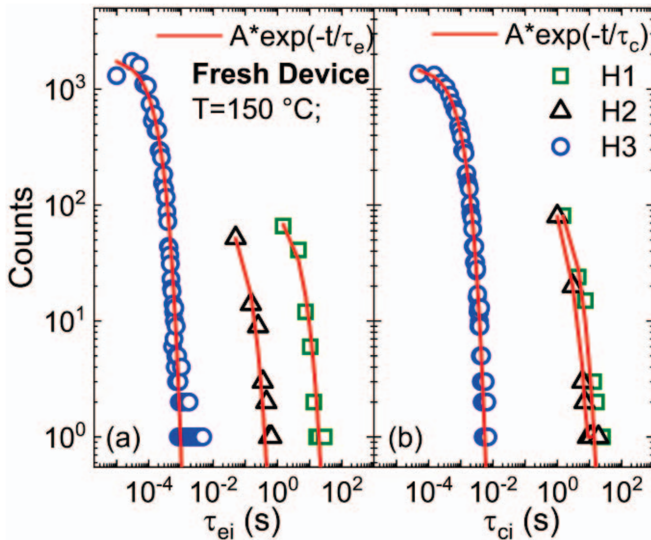

Figure 3. τ_e (a) and τ_c (b) from the discretized waveforms for the three RTN signatures detected at T=150 °C on fresh device.

From the two-state discretized signal of each RTN component, the charge emission time (τ_e) and capture time (τ_c), representing the time spent at the higher and lower current levels, respectively, are estimated. These times are extracted for each component and used to construct the corresponding distributions, as shown in Fig. 3(a) and 3(b). Exponential fitting is applied to derive the characteristic τ_e and τ_c for each defect state. It is important to note that both time constants exhibit an exponential distribution, indicative of a Poissonian process, common in charge trapping and de-trapping phenomena that lead to current fluctuations [24].

The cut-off time for each RTN component is calculated as follows:

$$\frac{1}{\tau_i} = \frac{1}{\tau_{e_i}} + \frac{1}{\tau_{c_i}} \quad (1)$$

This parameter represents the characteristic time associated with a defect and can be used to determine the related activation energy (Ea) and to reconstruct the power spectral density of the signal. In the PSD, RTN signatures are identified by segments exhibiting a $1/f^2$ trend, while the absence of such signature corresponds to a 1/f noise behavior.

The theoretical reconstruction of the signal in the frequency domain (PSD) is achieved by summing the Lorentzian spectra, one for each component. The equation is as follows:

$$PSD\ (f) = \sum_{i=1}^{N} \frac{(2 \cdot d_i \cdot \tau_i)^2}{(\tau_{e_i}+\tau_{c_i}) \cdot (1 + (2\pi \cdot f \cdot \tau_i)^2)} \quad (2)$$

N represents the number of $1/f^2$ components, which in this case is three. The parameters d_i and τ_i refer to the ith amplitude

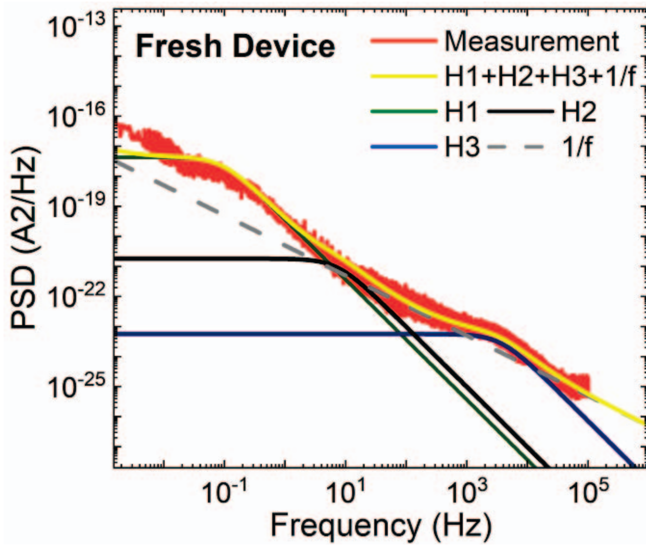

Figure 4. Measured (red) and reconstructed PSD (yellow) as a sum of Lorentzian spectra of the three RTN components at T=150 °C.

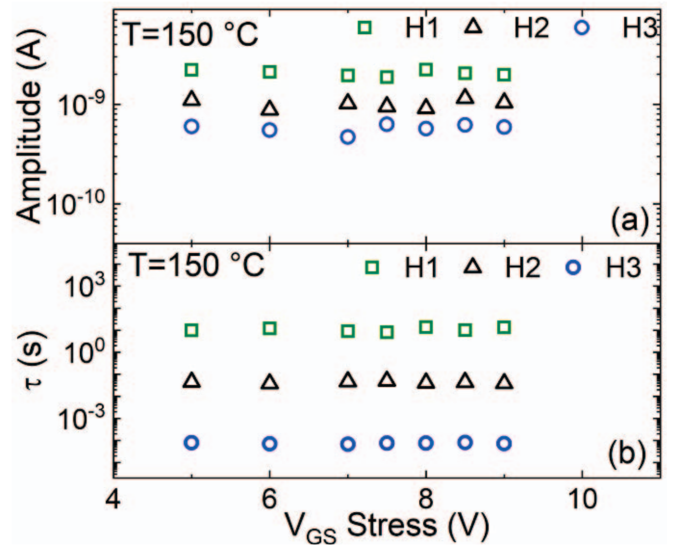

Figure 6. Amplitude (a) and cut-off time (b) as a function of V_{GS} for H1, H2 and H3 at T=150 °C.

of the RTN waveforms and the associated cut-off time (Eq. 1), respectively. The estimated amplitudes for the RTN components H1, H2, and H3 are 22 nA, 10.5 nA and 0.55 nA, respectively.

As shown in Fig. 4, the theoretical PSD, derived from Eq. 2, closely matches the measured data, validating the proposed analysis methodology. In contrast to the observations at room temperature [28], the sum of the three Lorentzian spectra here includes an additional 1/f noise component, which becomes significant at higher temperatures due to increased gate leakage.

The reconstructed PSDs from each PSM at T=150°C are reported in Fig. 5. Notably, RTN components are visible in the PSD from the initial monitoring phase of the fresh device through PSM5. However, in PSM6, no $1/f^2$ trend, indicative of RTN components, is observed. This absence corresponds to the higher and noisier gate current observed in Fig. 1 (b), which masks the RTN signature and makes its identification impossible.

Figures 6 (a) and (b) illustrate the dependence of RTN amplitude and time constant on V_{GS}, respectively. Notably, the RTNs remain consistent, exhibiting similar amplitude and τ, from the initial fresh measurement up to PSM5, indicating that no additional defects in the AlGaN barrier or at the Schottky junction are induced by forward gate stress. The absence of new defect creation, particularly at the Schottky junction (as observed at room temperature [28]), at elevated temperatures may be explained by the reduced influence of impact ionization (ii). The latter is known to contribute to the gate failure at lower temperatures [14], but its presence diminishes at higher temperatures. Furthermore, at 150 °C, breakdown in the isolation region of Schottky pGaN gate HEMTs occurs,

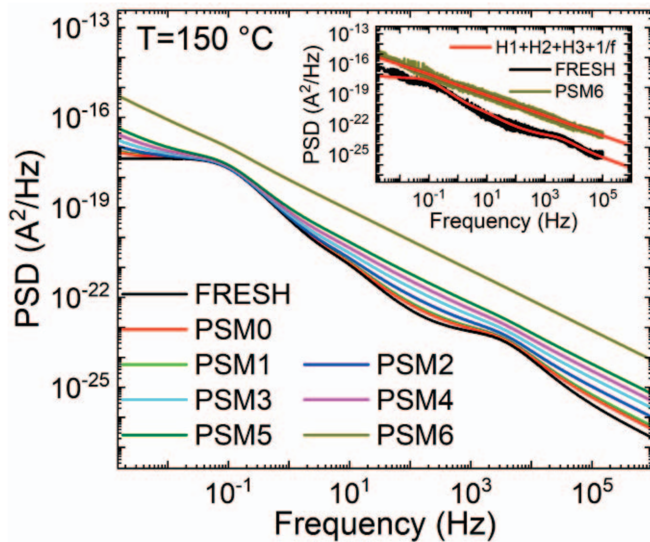

Figure 5. Reconstructed power spectral density for all the PSMs at T=150 °C. Inset: measured and reconstructed PSD for fresh and PSM6 I_G.

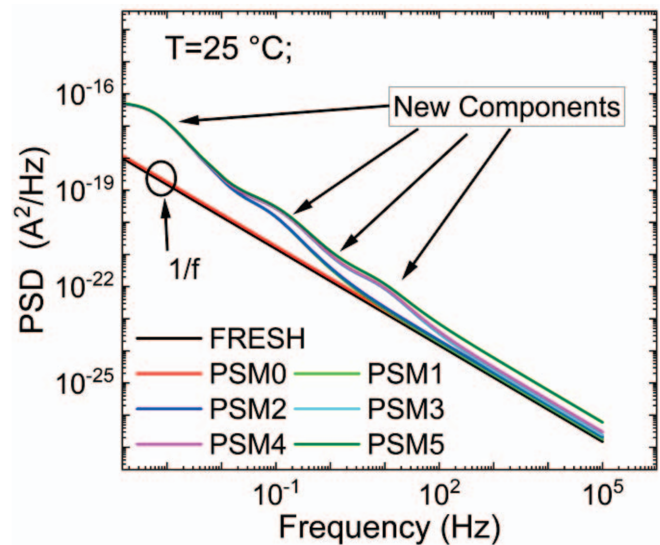

Figure 7. Reconstructed power spectral density for all the PSMs at T=25 °C.

possibly before any damage develops in the Schottky junction [14].

B. Room Temperature

A similar analysis has been performed at room temperature (T = 25 °C). Fig. 7 reports the reconstructed power spectral densities for all the PSMs. Notably, both the fresh and PSM0 show a 1/f slope, indicating the absence of RTN components under these conditions. In contrast, as the stressing V_{GS} increases, the PSD reveals new segments with a $1/f^2$ trend, indicative of the occurring of RTN components, suggesting the activation or creation of new defects.

A total of four distinct RTN components, labeled D1, D2, D3, and D4, have been identified across all experimental conditions. These components exhibit variations in amplitude and frequency, indicating the diverse properties of the associated defects. The observed RTN components are consistent with those previously reported in [28], with similar amplitudes and time constants. This consistency reinforces the conclusion that defect generation at T = 25 °C is governed by both the applied voltage and the stress duration. The time- and voltage-dependent nature of defect creation highlights the dynamic interplay between electrical stress and defect activation processes, providing critical insights into the underlying mechanisms contributing to device degradation under low-temperature operating conditions.

Defects D1, D2, and D3 are detected in both I_G and I_D, indicating the formation of new defects at varying locations within the AlGaN barrier. These defects likely contribute to threshold voltage shift by altering the barrier's electronic properties. In contrast, defect D4 is only observed in I_G, suggesting it originates in the Schottky depletion region. This localized defect formation is possibly associated with mechanisms that may lead to gate breakdown, distinguishing its behavior from that of the other defects.

The amplitude and time constant (Eq. 1) of these defects as functions of V_{GS} are shown in Fig. 8 (a) and (b), respectively, providing further insight into their characteristics and the influence of gate bias on their behavior. Specifically, the signatures of defects D1 and D2 first appear during PSM1, following the application of a stress condition at V_{GS}=7 V for 100 s. In contrast, defects D3 and D4 created or activated starting from PSM3. Once a defect appears, it remains detectable in all subsequent PSMs up to device breakdown, consistently exhibiting similar time constants and amplitudes across the measurements.

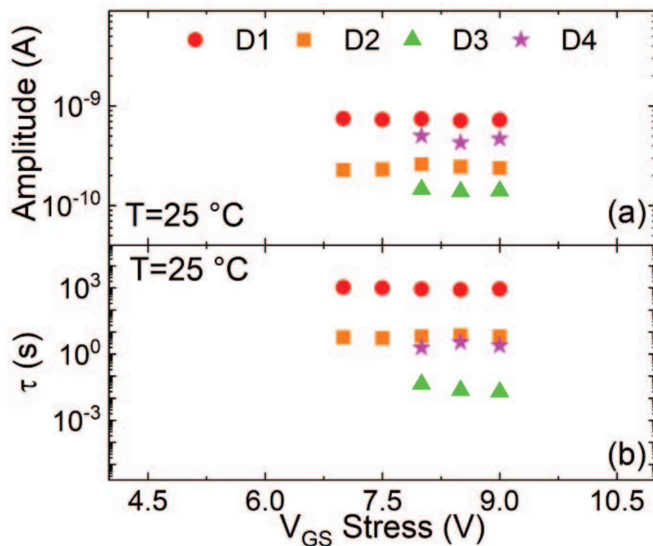

Figure 8. Amplitude (a) and characteristic time (b) as a function of V_{GS} for D1, D2, D3 and D4 at T=25 °C.

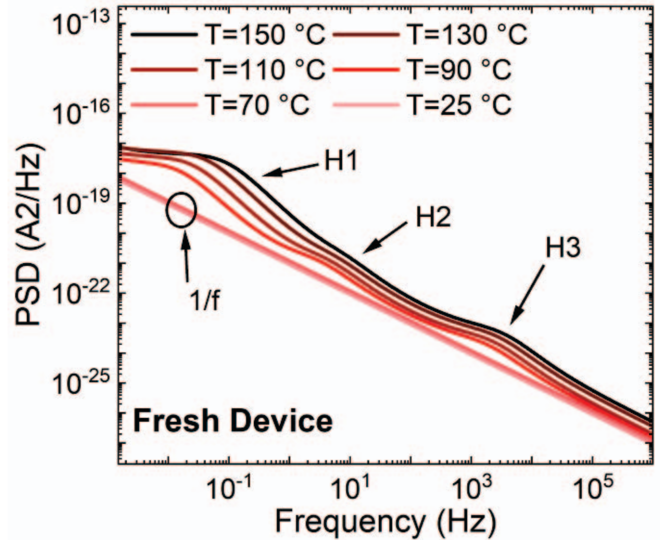

Figure 9. Reconstructed power spectral density for I_G monitored on the fresh device at different temperatures.

When comparing these findings with the previous analysis [28], it is clear that the activation or creation of defects D1 and D2 requires shorter stress times and lower voltage levels than defects D3 and D4. Specifically, defect D4's behavior further support the hypothesis that, at lower temperatures, gate breakdown in pGaN gate HEMTs is primarily driven by impact ionization occurring in the Schottky depletion region. This conclusion aligns with the established role of impact ionization in defects generation and eventual failure at low temperatures [14].

IV. Activation Energy Characterization

To gain a more comprehensive understanding of the pre-existing defects detected in the AlGaN barrier at T = 150 °C, the currents of fresh devices have been monitored across a temperature range from 25 °C to 150 °C. The reconstructed PSDs of the gate leakage corresponding to these measurements are shown in Fig. 9. It is worth noting that the RTN components labeled H1, H2, and H3 are clearly visible in the PSDs of the fresh device current within the temperature range of 90 °C to 150 °C. This indicates that fluctuations of similar amplitude are consistently detected within this range. In contrast, no RTN components are observed at temperatures below 70 °C, as the PSDs in this lower temperature range show a 1/f trend, indicative of the lack of observable RTN behavior.

This temperature-dependent behavior suggests that the activation of defects responsible for the RTN components H1, H2, and H3 is thermally driven. At T < 90 °C, the thermal energy may be insufficient to activate these defects, resulting in the absence of RTN signatures. As the temperature exceeds this threshold, the thermal activation of these defects becomes

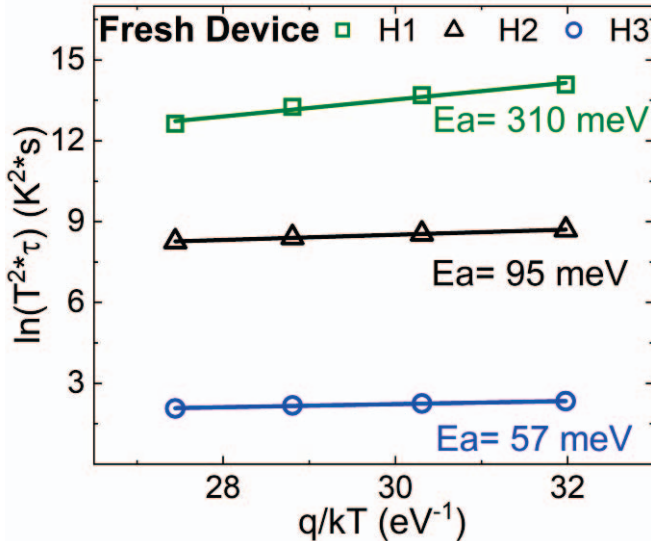

Figure 10. Arrhenius plot for the determination of the activation energy of H1, H2 and H3.

significant, leading to the appearance of distinct RTN components.

RTN analysis serves as a powerful tool for extracting key defect characteristics, particularly the activation energies (Ea) of individual defects, through the use of an Arrhenius plot (Fig. 10). By examining the temperature dependence of the cut-off time (i.e. the characteristic time of the traps), estimated following the procedure outlined in section III A, the activation energies of defects H1, H2, and H3 are found to be 310 meV, 95 meV, and 57 meV, respectively.

The observed differences in RTN amplitudes (Fig. 6a) and activation energies for H1, H2, and H3 highlight the presence of pre-existing defects located at distinct spatial positions and energy levels within the AlGaN barrier. These defects may arise from process imperfections or from mechanical stress induced by piezoelectric polarization at the AlGaN/GaN heterojunction. These findings provide critical insights into the structural and electronic properties of the AlGaN barrier.

V. Conclusions

This study has investigated Random Telegraph Noise to analyze the role of forward gate bias and temperature on defects activation and creation in the p-GaN/AlGaN/GaN epi-stack of Schottky p-GaN gate HEMTs.

RTN analysis at elevated temperatures ($T \geq 90$ °C) identified pre-existing defects in the AlGaN barrier, detected even on fresh devices. These defects, labeled H1, H2, and H3, influence the threshold voltage, as shown by fluctuations in both gate and drain currents. They exhibit distinct spatial locations and energy levels, and their role is visible only above 70 °C. The activation energies have been determined to be 310 meV, 95 meV, and 57 meV for H1, H2 and H3, respectively.

At lower temperatures ($T \leq 70$ °C), no pre-existing defects were detected. However, forward gate stress induced the formation of new defects, labeled D1, D2, D3 and D4. Defects D1 and D2 formed at lower stress levels, while D3 and D4 required higher voltages and longer stress durations [28].

Overall, this work demonstrated the utility of RTN as a powerful diagnostic tool for characterizing defect states in Schottky pGaN gate HEMTs. The findings provide valuable insights into how forward gate bias and temperature influence trapping/de-trapping mechanisms and device degradation.

References

[1] Pushpakaran, B.N., Subburaj, A.S. & Bayne, S.B. Commercial GaN-Based Power Electronic Systems: A Review. J. Electron. Mater. **49**, 6247–6262 (2020). https://doi.org/10.1007/s11664-020-08397-z.

[2] Koon Hoo Teo, Yuhao Zhang, Nadim Chowdhury, Shaloo Rakheja, Rui Ma, Qingyun Xie, Eiji Yagyu, Koji Yamanaka, Kexin Li, Tomás Palacios; Emerging GaN technologies for power, RF, digital, and quantum computing applications: Recent advances and prospects. *J. Appl. Phys.* 28 October 2021; 130 (16): 160902. https://doi.org/10.1063/5.0061555.

[3] W. Saito, "A Future Outlook of Power Devices From the Viewpoint of Power Electronics Trends," in *IEEE Transactions on Electron Devices*, vol. 71, no. 3, pp. 1356-1364, March 2024, doi: 10.1109/TED.2023.3332611.

[4] Zhang, Y., Udrea, F. & Wang, H. "Multidimensional device architectures for efficient power electronics." *Nat Electron* 5, 723–734 (2022). https://doi.org/10.1038/s41928-022-00860-5.

[5] Y. Wu, M. Jacob-Mitos, M. L. Moore and S. Heikman, "A 97.8% Efficient GaN HEMT Boost Converter With 300-W Output Power at 1 MHz," in *IEEE Electron Device Letters*, vol. 29, no. 8, pp. 824-826, Aug. 2008, doi: 10.1109/LED.2008.2000921.

[6] J. P. Kozak *et al.*, "Stability, Reliability, and Robustness of GaN Power Devices: A Review," in *IEEE Transactions on Power Electronics*, vol. 38, no. 7, pp. 8442-8471, July 2023, doi: 10.1109/TPEL.2023.3266365.

[7] A. N. Tallarico *et al.*, "PBTI in GaN-HEMTs With p-Type Gate: Role of the Aluminum Content on ΔV_{TH} and Underlying Degradation Mechanisms," in *IEEE Transactions on Electron Devices*, vol. 65, no. 1, pp. 38-44, Jan. 2018, doi: 10.1109/TED.2017.2769167.

[8] S. -W. Tang *et al.*, "Using Gate Leakage Conduction to Understand Positive Gate Bias Induced Threshold Voltage Shift in p-GaN Gate HEMTs," in *IEEE Transactions on Electron Devices*, vol. 70, no. 2, pp. 449-453, Feb. 2023, doi: 10.1109/TED.2022.3231566.

[9] A. N. Tallarico *et al.*, "P-GaN Gate HEMTs: A Solution to Improve the High-Temperature Gate Lifetime," in *IEEE Electron Device Letters*, vol. 45, no. 9, pp. 1630-1633, Sept. 2024, doi: 10.1109/LED.2024.3424563.

[10] L. Sayadi, G. Iannaccone, S. Sicre, O. Häberlen and G. Curatola, "Threshold Voltage Instability in p-GaN Gate AlGaN/GaN HFETs," in *IEEE Transactions on Electron Devices*, vol. 65, no. 6, pp. 2454-2460, June 2018, doi: 10.1109/TED.2018.2828702.

[11] X. Chao *et al.*, "Analysis of V_{TH} Degradation and Recovery Behaviors of p-GaN Gate HEMTs Under Forward Gate Bias," in *IEEE Transactions on Electron Devices*, vol. 70, no. 6, pp. 2970-2974, June 2023, doi: 10.1109/TED.2023.3263819.

[12] X. Tang, B. Li, H. A. Moghadam, P. Tanner, J. Han and S. Dimitrijev, "Mechanism of Threshold Voltage Shift in *p*-GaN Gate AlGaN/GaN Transistors," in *IEEE Electron Device Letters*, vol. 39, no. 8, pp. 1145-1148, Aug. 2018, doi: 10.1109/LED.2018.2847669.

[13] I. Rossetto *et al.*, "Time-Dependent Failure of GaN-on-Si Power HEMTs With p-GaN Gate," in *IEEE Transactions on Electron Devices*, vol. 63, no. 6, pp. 2334-2339, June 2016, doi: 10.1109/TED.2016.2553721.

[14] M. Millesimo *et al.*, "High-Temperature Time-Dependent Gate Breakdown of p-GaN HEMTs," in *IEEE Transactions on Electron Devices*, vol. 68, no. 11, pp. 5701-5706, Nov. 2021, doi: 10.1109/TED.2021.3111144.

[15] S. Yang *et al.*, "Identification of Trap States in p-GaN Layer of a p-GaN/AlGaN/GaN Power HEMT Structure by Deep-Level Transient Spectroscopy," in *IEEE Electron Device Letters*, vol. 41, no. 5, pp. 685-688, May 2020, doi: 10.1109/LED.2020.2980150.

[16] S. Pan *et al.*, "Evaluation of Trapping Behaviors in Forward Biased Schottky-Type p-GaN Gate HEMTs," in *IEEE Transactions on Electron Devices*, vol. 70, no. 7, pp. 3475-3482, July 2023, doi: 10.1109/TED.2023.3278614.

[17] M. Millesimo *et al*., "Role of the GaN-on-Si Epi-Stack on ΔR_{ON} Caused by Back-Gating Stress," in *IEEE Transactions on Electron Devices*, vol. 70, no. 10, pp. 5203-5209, Oct. 2023, doi: 10.1109/TED.2023.3304272.

[18] Huake Su, Tao Zhang, Shengrui Xu, Hongchang Tao, Boxiang Yun, Jincheng Zhang, Yue Hao, "Interface state analysis of Schottky-gated p-AlGaN/u-GaN/AlGaN p-FET with negligible hysteresis at high temperatures." *Appl. Phys. Lett.* 25 September 2023; 123 (13): 132104, doi: 10.1063/5.0156040.

[19] S. Realov and K. L. Shepard, "Random telegraph noise in 45-nm CMOS: Analysis using an on-chip test and measurement system," *2010 International Electron Devices Meeting*, San Francisco, CA, USA, 2010, pp. 28.2.1-28.2.4, doi: 10.1109/IEDM.2010.5703436.

[20] M. Luo, R. Wang, S. Guo, J. Wang, J. Zou and R. Huang, "Impacts of Random Telegraph Noise (RTN) on Digital Circuits," in *IEEE Transactions on Electron Devices*, vol. 62, no. 6, pp. 1725-1732, June 2015, doi: 10.1109/TED.2014.2368191.

[21] B. H. Hong *et al*., "Temperature Dependent Study of Random Telegraph Noise in Gate-All-Around PMOS Silicon Nanowire Field-Effect Transistors," in *IEEE Transactions on Nanotechnology*, vol. 9, no. 6, pp. 754-758, Nov. 2010, doi: 10.1109/TNANO.2010.2045006.

[22] N. Conrad *et al*., "Low-frequency noise and RTN on near-ballistic III–V GAA nanowire MOSFETs," *2014 IEEE International Electron Devices Meeting*, San Francisco, CA, USA, 2014, pp. 20.1.1-20.1.4, doi: 10.1109/IEDM.2014.7047086.

[23] F. M. Puglisi, P. Pavan, A. Padovani, L. Larcher, and G. Bersuker, "RTS noise characterization of HfOx RRAM in high resistive state," Solid-State Electron., vol. 84, pp. 160–166, Jun. 2013, doi: 10.1016/j.sse.2013.02.023.

[24] F. M. Puglisi and P. Pavan, "Guidelines for a Reliable Analysis of Random Telegraph Noise in Electronic Devices," in *IEEE Transactions on Instrumentation and Measurement*, vol. 65, no. 6, pp. 1435-1442, June 2016, doi: 10.1109/TIM.2016.2518880.

[25] E. Simoen, B. Dierickx, C. L. Claeys and G. J. Declerck, "Explaining the amplitude of RTS noise in submicrometer MOSFETs," in *IEEE Transactions on Electron Devices*, vol. 39, no. 2, pp. 422-429, Feb. 1992, doi: 10.1109/16.121702.

[26] T. Grasser, K. Rott, H. Reisinger, M. Waltl, J. Franco and B. Kaczer, "A unified perspective of RTN and BTI," *2014 IEEE International Reliability Physics Symposium*, Waikoloa, HI, USA, 2014, pp. 4A.5.1-4A.5.7, doi: 10.1109/IRPS.2014.6860643.

[27] J. -H. Bae *et al*., "Analysis of DC/transient current and RTN behaviors related to traps in p-GaN gate HEMT," *2013 IEEE International Electron Devices Meeting*, Washington, DC, USA, 2013, pp. 31.6.1-31.6.4, doi: 10.1109/IEDM.2013.6724733.

[28] M. Millesimo *et al*., "Analysis of RTN Induced by Forward Gate Stress in GaN HEMTs with a Schottky p-GaN Gate," *2024 IEEE International Reliability Physics Symposium (IRPS)*, Grapevine, TX, USA, 2024, pp. 1-6, doi: 10.1109/IRPS48228.2024.10529393.